PassiveLiFi: Rethinking LiFi for Low-Power and Long Range RF Backscatter

Muhammad Sarmad Mir
IMDEA Networks
Universidad Carlos III de Madrid
Madrid, Spain
sarmad.mir@imdea.org

Borja Genoves Guzman
IMDEA Networks
Madrid, Spain
borja.genoves@imdea.org

Ambuj Varshney
Uppsala University
Uppsala, Sweden
ambujvarshney@acm.org

Domenico Giustiniano
IMDEA Networks
Madrid, Spain
domenico.giustiniano@imdea.org

ABSTRACT

Light bulbs have been recently explored to design Light Fidelity (LiFi) communication to battery-free tags, thus complementing Radiofrequency (RF) backscatter in the uplink. In this paper, we show that LiFi and RF backscatter are complementary and have unexplored interactions. We introduce PassiveLiFi, a battery-free system that uses LiFi to transmit RF backscatter at a meagre power budget. We address several challenges on the system design in the LiFi transmitter, the tag and the RF receiver. We design the first LiFi transmitter that implements a chirp spread spectrum (CSS) using the visible light spectrum. We use a small bank of solar cells for communication and harvesting and reconfigure them based on the amount of harvested energy and desired data rate. We further alleviate the low responsiveness of solar cells with a new low-power receiver design in the tag. Experimental results with an RF carrier of 17 dBm show that we can generate RF backscatter with a range of 80.3 meters/μW consumed in the tag, which is almost double with respect to prior work.

CCS CONCEPTS

• **Computer systems organization** → **Sensor networks**; • **Hardware** → *Networking hardware*; *Sensor devices and platforms*; *Wireless devices.*

ACM Reference Format:
Muhammad Sarmad Mir, Borja Genoves Guzman, Ambuj Varshney, and Domenico Giustiniano. 2022. PassiveLiFi: Rethinking LiFi for Low-Power and Long Range RF Backscatter. In *The 27th Annual International Conference on Mobile Computing and Networking (ACM MobiCom '21), January 31-February 4, 2022, New Orleans, LA, USA.* ACM, New York, NY, USA, 13 pages. https://doi.org/10.1145/3447993.3483262

*Ambuj Varshney is presently a Postdoctoral scholar with UC Berkeley (EECS)

ACM MobiCom '21, January 31-February 4, 2022, New Orleans, LA, USA

ACM ISBN 978-1-4503-8342-4/22/01…$15.00
https://doi.org/10.1145/3447993.3483262

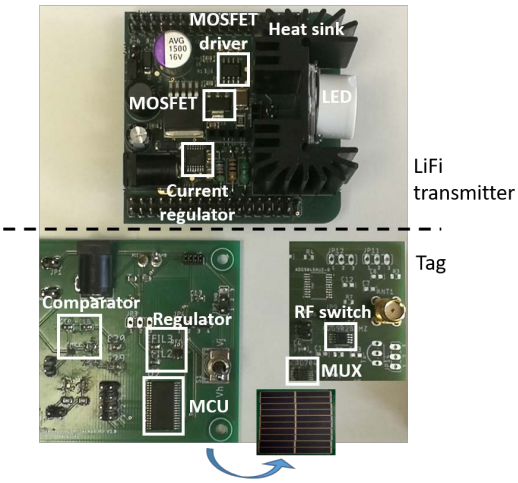

Figure 1: PassiveLiFi: hardware prototypes of LiFi transmitter and passive tag. The tag comprises LiFi module for downlink (backside), solar cell array for energy harvesting and downlink communication (frontside), and RF backscatter module for uplink.

1 INTRODUCTION

The large scale deployment of Internet of Things (IoT) devices leads to massive use of batteries, as they provide energy to IoT devices. Although batteries in tiny form factor may last for a long time, even years, any computation and communication can quickly deplete them, and it calls for solutions that do not need batteries at all. Additionally, batteries have also a negative environmental impact, as consumers currently dispose of billions of batteries per year and battery recycling is a delicate matter [6, 36].

The research efforts in battery-free systems exploits low-power electronics, communication and processing techniques [8, 19, 35, 40]. RF backscatter is now a consolidated technology for transmitting IoT data to the network because of its energy efficiency and absence of power-hungry active radio for transmission. In fact, the scarce amount of harvested energy from the environment limits the communication and processing capabilities. In particular, energy is mainly harvested from RF [32], light [8, 40, 44] and kinetic [14] sources. A solar cell is typically used for harvesting energy from

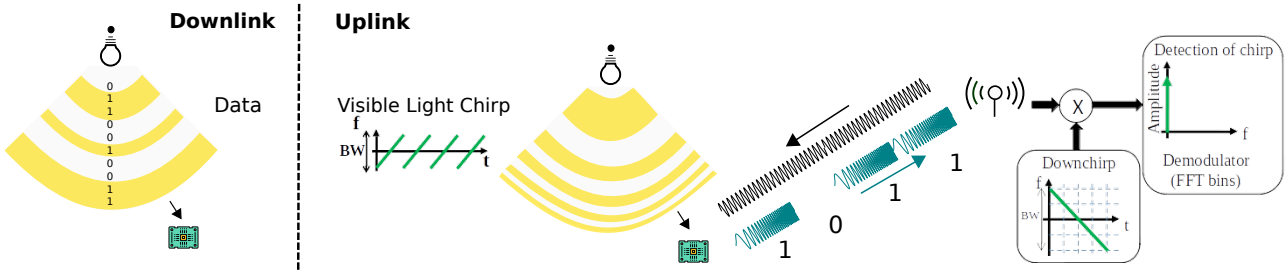

Figure 2: Downlink (left): Light intensity is changed to send data to passive tag at a fixed clock rate. Uplink (right): Carrier and baseband delegated to the infrastructure. Chirps are complex to generate at the tag, and hence we delegate them to the light infrastructure. The light intensity is changed to generate visible light chirp at a varying clock rate. This chirp is then mixed in the tag with the input RF carrier for RF backscatter.

light, and it provides the best trade-off between the level of energy provided and the availability of sources [12, 45].

Only limited work has been conducted to exploit commodity solar cells in battery-free IoT devices also for communication. EDISON [12] has shown the design of a battery-free IoT tag that receives data through light, a concept commonly called Visible Light Communication (VLC) or Light Fidelity (LiFi) in a networked system. It then sends data through RF backscatter. It achieved an uplink range of about 20 m indoors, co-locating the RF receiver with the LiFi bulb, and consuming 70 μW of energy for uplink communication. EDISON demonstrated that LiFi and RF backscatter are incomplete as standalone technologies for passive communication, but have *complementary properties* that can be exploited to use LiFi in downlink and RF backscatter in uplink.

In this work, we introduce PassiveLiFi, shown in Fig. 1, which exploits the *unexplored interactions* between LiFi communication in downlink and RF backscatter in uplink. As we will show in this work, these interactions allow us to significantly increase both the range for RF backscatter and the energy efficiency of the IoT tag. We use LiFi not only to transmit downlink data, but also to generate the clock signal needed by the IoT tag to transmit RF backscatter in uplink, thus removing the need of a clock in the IoT tag. A first approach could be to modulate the LiFi bulb with a simple On-Off Keying (OOK) modulation and use this signal as clock in the IoT tag. This approach would already result in energy saving in the IoT tag. However the RF backscatter communication range would be similar to the traditional design that uses oscillators in the IoT tag for the same purpose [12]. In order to increase both the communication range in RF backscatter and decode signals drowned by the noise, we present the first implementation of chirp spread spectrum (CSS) using the visible light spectrum. This visible light signal is received by the solar cells in the IoT tag, and used there as baseband signal to communicate with RF backscatter by turning the chirp on and off based on the bit stream. Generating chirp spread spectrum in the tag consumes around 10 mW using off-the-shelf components [34], and offloading it to the infrastructure while completely removing the need of oscillators for passive chirp spread spectrum has been not shown so far. A high level illustration of PassiveLiFi is presented in Fig. 2, where we show the operations both in downlink and uplink.

A first problem we have to solve in order to implement chirp spread spectrum in LiFi is that commercial light bulbs could modulate the light intensity at speeds in the order of a few Mb/s. However, solar cells have not been designed for communication, and thus they have inefficiencies as receivers that must be addressed to sustain sufficient high data rate. Furthermore, delegating chirp generation to the infrastructure requires that the LiFi receiver in the IoT tag consumes low power, smaller than the one consumed by the local oscillators for performing CSS modulation. Yet, low-power LiFi receivers are based on light power envelope and are sensitive to any source of light interference, like other light fixtures and sun.

A second problem is that prior work used two different solar cells, one for communication and one for harvesting [12]. However, this has two drawbacks: it increases the size of tag or, if we keep the same tag area, it does not exploit all available light energy for both communication and harvesting. Besides, solar cells are typically designed to work with solar energy, but its effectiveness with indoor and artificial lighting conditions is less known.

Our contributions can be summarized as follows.

- We present the first design of chirp spread spectrum using LiFi, and propose to use LiFi in two modes of operation: the first one for communicating downlink data, and the second one for generating the chirp signal needed by uplink RF backscatter. In the first mode, it uses a traditional constant clock rate, while, in the second mode, the clock rate changes based on the desired bandwidth and spreading factor;
- We propose a design that uses a single solar cell both for communication and harvesting, decoupling the modulated LiFi signals received from light bulbs from the light energy that can be used for harvesting. We show that the problem of optimizing both communication and harvesting with a solar cell follows a Pareto curve and we propose a criterion to select the best solar cells for both communication and harvesting;
- We implement PassiveLiFi with customized hardware both on the LiFi transmitter and IoT tag, and we evaluate our system in a variety of scenarios. Our experiments show that PassiveLiFi can transmit RF backscatter signals with a meter/power consumed metric that is almost doubled with respect to the state of the art.

The rest of the paper is structured as follows: In Section 2, we present challenges faced by state-of-the-art systems, and we place our system in context to them. We also provide a high-level overview of our system. Next, in the Sections 3 and 4, we describe the design of the LiFi transmitter and the tag. We describe in detail the operation of our system. In Section 5 we evaluate the system in terms of range, energy harvesting and power consumption in different scenarios. Next, in Section 6, we present application scenarios that

our system could enable. Finally, we discuss prior works related to our system, and we conclude the paper.

2 CHALLENGES

We discuss the challenges we address in this work and position them with respect to prior work in the literature.

2.1 Delegating oscillators

RF backscatter absorbs and reflects the surrounding radio waves to communicate with battery-free devices. On these devices, achieving low energy consumption for every device is essential to enable its operation on the small amounts of energy harvested from the ambient environment. On the backscatter tags, the oscillator's energy dominates the overall energy consumption, and it is the order of tens of μWs (demonstrated through simulation or implementation [31]). Further, these oscillators are often combined with other circuits such as those to generate chirps for communication, which further pushes the complexity and energy consumption [29]. It makes it prohibitive to operate these platforms on the harvested energy. Recent systems overcome the oscillators' energy-expensive nature by delegating oscillations to an external and powered RF infrastructure [31]. This leads to lowering the power consumption and complexity of the backscatter tag. However, the communication range is not sufficient for most applications, and it is in the order of 2 m. One possible approach to increase the communication range is to employ chirps for communication. However, generating these chirps locally at the tag is an energy-expensive operation. Prior work has also tried to delegate the energy-expensive process of generating chirps [29]. However, it still required an oscillator at the tag to shift this signal by 1-2 MHz to avoid self-interference and backscatter it back to the RF receiver. This leads to an increased complexity and power consumption of the backscatter tag.

Offloading chirp spread spectrum signals to the infrastructure while completely removing the need of oscillators for passive chirp spread spectrum has been not shown so far. Yet, the ability to offload chirp signals could result in a much larger communication range than using simpler modulations which are prone to error [17]. Delegating oscillations to the infrastructure requires that the power budget needed for downlink reception in the tag is lower than the one consumed by its local oscillators. Furthermore, the received signal must be also sufficiently precise to be used as oscillator. This is difficult to achieve because of the limitation of passive envelope detectors, commonly used as RF receivers in tags. In fact, passive envelope detectors aggregate all energy received in the band, and cannot select a desired frequency as clock. Besides, any ambient traffic could trigger simple RF envelope detectors, increasing the consumption of the tag [12].

Instead of delegating the chirp spread spectrum to the RF infrastructure, we propose to use light bulbs for generating *visible light chirps* that can be detected by low power LiFi receivers. These receivers can provide better baseband signals than their RF counterparts for two reasons:

- LiFi transmission follows an Intensity Modulation (IM) baseband procedure, where the modulation of the optical power of the LiFi transmission carries the information, and the signal phase does not carry the information. Instead, the receiver carries out a Direct Detection (DD) to convert the optical received signal into an electrical signal. In its simplest form, LiFi requires to just turn on and off the Light Emitting Diode (LED) in the bulb with the desired pattern to transmit a bit stream. We instead cannot send RF signals in the baseband and they require an RF carrier.
- Passive LiFi receivers can be designed with low-power consumption, yet the light propagation can be much better controlled than the RF propagation. Light is more confined than RF and, as a consequence, LiFi receivers may receive fewer interfering signals. The main source of interference is the sunlight, which is not modulated, and therefore can be filtered out at the receiver, and other sources from older technologies, such as fluorescent lights, are disappearing.

2.2 Communication and harvesting

In passive LiFi systems, the receiver relies on solar cells both for communication and harvesting. Solar cells are advantageous with respect to other optical receivers such as photodiodes because they operate fully passive, without the usage of any active amplifier [12]. In order to use the overall light sensitive area, we advocate for a design that uses the same solar cell for both communication and harvesting. A simple approach would be to slice the time such that a certain portion of time is dedicated to harvesting and the rest to communication. However, this would result in poor efficiency. More formally, let us define T_c as the time to communicate N bits and T_h as the time to harvest enough energy to transmit N bits. Because of the latency required for harvesting, the time left for a single battery-free device to communicate data would be largely reduced and T_c would increase significantly. Furthermore, the time needed to harvest energy could disrupt any protocol that needs to use the same solar cell for communication.

Rather than using the same solar cell in different slices of time, we aim to use it *at the same time* both for communication and harvesting, without losing any energy that could be useful for harvesting. However, the photonics community has always considered this unrealistic because of how photodetectors (and solar cells are just one type of them) work. Fundamentally, in order to receive data, photodetectors are bias in reverse mode, meaning that there is a higher voltage to the negative pin with respect to the positive pin of the photodetector. In contrast, when the photodetector operates in photovoltaic mode to harvest energy, it is positive bias, and hence the voltage is with opposite sign with respect to communication mode. In this work, we present a new low-power LiFi receiver to solve this problem, leveraging the fact that communication and harvesting use different frequency components of the same signal. Therefore, we take as input the voltage signal given by the solar cell, and disentangles it into two components, one for harvesting and another for communication. We further propose to use a small set of solar cells instead of a single larger one to optimize communication and harvesting depending on the needs.

In what follows, we address the limitations presented in this section for low-power battery-free devices and present PassiveLiFi, composed of:

- LiFi transmitter to communicate to the tag and generate the baseband signal for uplink communication (Section 3);
- battery-free tag to receive and process LiFi signal, harvest energy from the solar cells, and provide uplink mixing the input

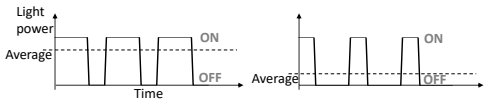

(a) LED for light dimming.

(b) LED as communication source.

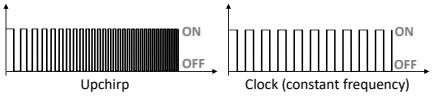

(c) LED as clock generator.

Figure 3: Varying LED intensity can serve multiple requirements. Its first application was light dimming (a); with LiFi, it has been used to transmit downlink data (b); in this work we propose to use it as clock generator, varying its frequency over time, to generate the baseband signal for uplink communication (c).

RF carrier and the LiFi baseband signal for RF backscatter communication (Section 4);

The system is complemented by the RF infrastructure to provide carrier signal for RF backscatter and process the received backscatter signal.

3 LIFI TRANSMITTER

In PassiveLiFi, the LiFi transmitter provides the illumination to fulfill the requirements of indoor lighting standards. It provides the energy to the tag to support battery-free operation for indoor deployments, and the baseband signals to support downlink communication and oscillations to support the RF backscatter-based uplink channel. The prototype we have built of the LiFi transmitter is shown on the top of Fig. 1.

3.1 Multiple roles of light bulbs

We are observing a rapid deployment of LED lighting in homes, offices and streetlights because of their energy efficiency and long lifespan. We refer to Fig. 3. Typically LEDs are driven by a switching power circuitry that operates at high frequency. This driver has been first used for light dimming by controlling the amount of time the light is on with respect to the time is off[1]. More recently, LEDs have started to be employed to generate LiFi signals, where the intensity of light is modulated to convey information. In its simplest form, LiFi communication associates bit 1 to high light intensity and bit 0 to low light intensity. In turn, a baseband signal is emitted by the bulb in the visible spectrum.

In this work, we propose to change the light intensity of LED bulbs for a third purpose, suitable for creating passive LiFi communication. We create a baseband signal with LiFi that can be mixed at the IoT tag with a RF carrier signal. This super-imposed signal can then be modulated by the tag, simply turning on and off the RF signal that is reflected. This clock signal can be used to offload

[1]Pulse width modulation is typically used for this purpose.

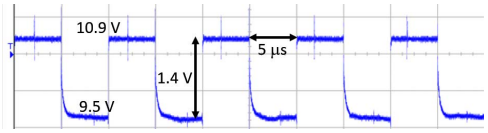

(a) OpenVLC transmit signals.

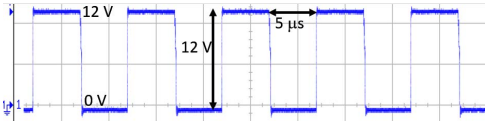

(b) New LiFi TX signals.

Figure 4: Comparison of 100 kHz signals transmitted by OpenVLC1.3 (only 10.9-9.5=1.4 Vpp and also with relevant capacitance effect) and our LiFi (peak-to-peak voltage is 12 V, with a very sharp waveform).

the oscillator in the IoT tag to the LiFi transmitter. One key advantage of this approach is the energy saving in the IoT tag thanks to offloading of the oscillator to the LiFi transmitter and removal of power-hungry elements on the tag.

3.2 Bandwidth in passive downlink

As discussed in Section 2.1, passive downlink communication requires a very low-power receiver. Any distortion in the signal received by the tag could inevitably cause errors in the interpretation of the bit pattern. We study this problem measuring the signal transmitted using the open source and low-cost OpenVLC1.3 board [11]. This platform has been also used by EDISON as LiFi transmitter. We transmit a 100 kHz signal using OpenVLC1.3, measure the voltage at the LED pins and plot the result in Fig. 4. We observe that the shape of transmitter signal distorts at higher frequencies, with a transient time from 90% to 10% of about 0.8 μs, which is 16% of the duration of one bit.

An active receiver could easily handle this transition time and operate up to 1 Msample/sec (as shown in OpenVLC [11]). On the contrary, passive LiFi communication requires a baseband signal as sharp as possible, such that a simple comparator of light intensity could be effective to distinguish high and low light intensity. Another problem is that OpenVLC operates the LED at low forward voltage of 10.9 V and current of 175 mA. As the relation between LED current and the output luminous flux is approximately linear, this design leads to poor harvesting and communication capabilities.

We modify the OpenVLC design with the goal of achieving a sharper baseband signal with low-cost hardware, and exploit the full dynamic range of the LED. We use the same LED as in OpenVLC, but we largely improve the front-end design. We increase the harvesting capabilities and range of communication operating the LED at higher forward voltage. OpenVLC uses a resistance in series to the LED, which wastes energy, and it cannot work at higher current levels. We instead use switching regulator based LED transmitter design, widely used for commercial LED luminaries. This allows us to operate the same LED at the highest current possible (550 mA), provide sharper transmitted signal at higher frequencies and dissipate only 10% energy as heat and switching losses, contrary to 51.6% for linear regulator such as OpenVLC1.3.

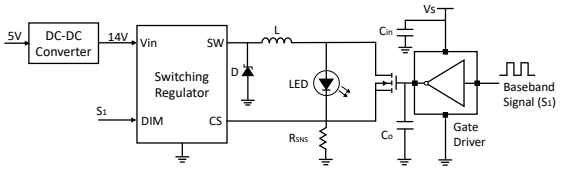

(a) LiFi transmitter design.

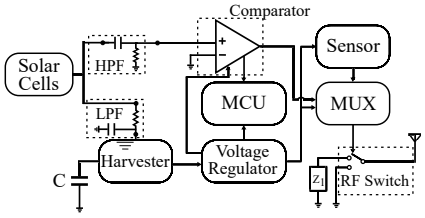

(b) Block diagram of battery-free IoT tag.

Figure 5: LiFi transmitter and battery-free IoT tag.

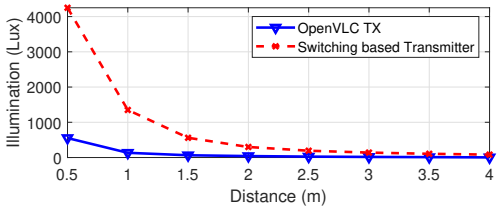

Figure 6: Comparison of illumination provided by OpenVLC TX and our design. Illuminance is multiplied by 10 at a distance of 1 m (1350 lux vs. 134 lux) and larger distance can be achieved while illuminating at typical illuminance values.

The schematic of our LiFi transmitter is shown in Fig. 5a, and the hardware prototype in Fig. 1. The regulator that we use operates in continuous conduction mode to maintain positive current through the inductor L and rectifies the biggest delay in turning the LED on and off. The parallel N-channel MOSFET is used to increase the slew rate of LED to achieve high switching frequency. The MOSFET gate driver is used to provide high current in order to overcome the effect of gate capacitance in high switching frequencies required to generate the chirp signal.

We outperform OpenVLC design. From our tests, we observe that setting V_s at 5V, we achieve a sharper signal across the LED, as it can be seen in Fig 4. The experiments in Fig. 6 show that the measured illuminance with a luxmeter is multiplied by 10 at a distance of 1 m with respect to OpenVLC, enabling larger scenarios with LED lighting [20].

3.3 Visible light chirps

As discussed in Section 2.1, we propose to use light bulbs for delegating oscillations. For instance, with PassiveLiFi, we can generate the RF signal at 880 MHz and the LiFi signal at 100 kHz. The IoT tag can passively mix them to generate an operation frequency of 880.1 MHz for the uplink RF communication. Yet, this approach would improve only the energy efficiency, but not the range of communication.

Instead we propose to delegate the generation of chirp signals to LiFi, as shown in Fig. 2. Chirp spread spectrum (CSS) can achieve longer range with respect to simpler modulations (e.g., On-Off keying), as successfully shown in LoRa [1] thanks to the property below

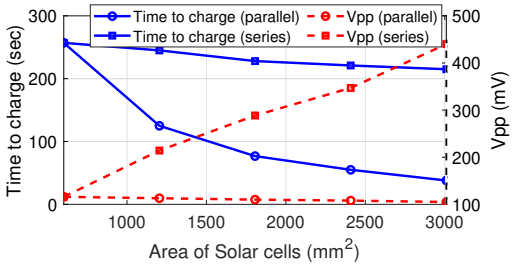

Figure 7: Effect of solar cell area on communication and harvesting using up to five solar cells in parallel or series. The energy harvesting ability improves when the solar cells are connected in parallel. Whereas, when the solar cells are connected in series, the ability to receive downlink communication is enhanced.

CSS to demodulate signals below the noise level, being also more robust to multipath. We propose to use light bulbs for generating visible light chirps, with the objective of improving both energy efficiency and range of uplink communication. In PassiveLiFi, the LiFi transmitter sends a clock with varying frequency over the visible light channel that increases over time (up-chirp signal). Note that there is no light flicker with our implementation of CSS as we work at sufficient high frequency, starting from 40 kHz. Next, the tag receives these transmissions using low-power solar cell-based LiFi receiver and further modulates the signal based on the information to be transmitted. On the receiver side, symbols are detected by the energy observed at different FFT bins, correlating the received signal with a down-chirp signal (cf. Fig. 2).

4 IOT TAG

The core of our end-to-end communication system is the battery-free IoT tag. The tag operates solely on harvested energy from solar cell. Solar cells are preferred for harvesting because of the widespread availability of light sources and higher level of harvested energy with respect to RF [45]. RF sources are also limited in space and deploying dedicated RF source has practicality issues. Furthermore, high RF power sources are needed to achieve reasonable harvesting (3 W transmitters to achieve less than 200 μW of power harvested at 5 m [24]). For the solar cells, we consider a total size of 30 cm^2 (4.6 inch^2), which is similar or smaller with respect to the state of the art [8, 12, 40].

The design goals for the tag include:

- Use of single solar cell for both harvesting energy and downlink communication;
- Energy thresholding circuit design in the tag robust to indoor lighting and LiFi communication frequency;
- Use of downlink chirp signal to enable long-range and low-power uplink backscatter communication;
- Ultra low-power design to enable maximum operation time on harvested energy.

The block diagram of the IoT tag is shown in Fig. 5b.

4.1 Trade-offs with solar cells

In this work, we propose to use a small set of solar cells instead of a single larger one, and use all of them for both harvesting and communication. Yet, we find that there exists a dichotomy between harvesting and communication that we have to solve. We perform

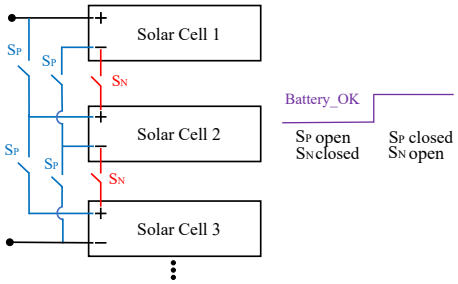

Figure 8: Combination of solar cell array in series or parallel depending on the charge level of battery/capacitor.

an experiment where we measure the time the solar cell takes to charge a capacitor of a specific value, time to charge (T_c) as well as the peak-to-peak value of the voltage measured at the receiver after the solar cells (V_{pp}). The experiment is performed at a distance of 1.5 m between our LiFi transmitter and receiver at 50 kHz frequency without background light.

We need small time to charge (we can harvest more quickly) and a high V_{pp} (we can operate at longer range). As represented in Fig. 7, this can be obtained using a larger total area of the solar cells, thus using all solar cells for both harvesting and communication. However, the harvesting improves considerably (time-to-charge decreases) with multiple (up to five) solar cells connected in parallel, while the communication worsens slightly, due to a lower V_{pp} value. On the other hand, when multiple solar cells are connected in series, the communication is boosted (larger V_{pp}) and the time-to-charge slightly decreases.

4.2 Reconfiguring the solar cells

The decision of parallel or series connection of solar cells is based on V_{BAT} which is the voltage across the capacitor to store harvested energy. The harvester BQ25570 generates a Battery_OK digital signal depending on the state of V_{BAT}. When V_{BAT} is above threshold (programmable by resistors), the Battery_OK is high and it toggles when V_{BAT} drops below the threshold. The configuration of solar cells can be switched between series and parallel by connecting the Battery_OK signal to gates of N-channel MOSFETs (S_N) and P-channels MOSFETs (S_P) as shown in Fig. 8. We need 'n-1' N-channel and '2n-2' P-channel MOSFETs for the design where 'n' is the number of solar cells used. ADG72X [4] switches can be used due to their low power dissipation (< 0.1 µW) and tiny package. In this way, connection among solar cells is reconfigurable automatically: when harvesting is the priority due to low charge on capacitor, solar cells are connected in parallel; when harvesting is not priority, to boost the communication they are connected in series. Note that, although harvesting or communication is being prioritized each time, both actions occurs simultaneously.

4.3 Comparison of commodity solar cells

There exist several solar cells in the market for IoT applications, and we study how to select the best performing solar cell in terms of harvesting and communication performance. Although solar cells in the market are all low cost (4-5 dollars each), their efficiency for harvesting varies largely (from 3 to 25%) as well as their size. Specifications of the communication performance are not given, as solar cells are designed typically only for harvesting. We study a total of six different commodity solar cells, and shortlisted three

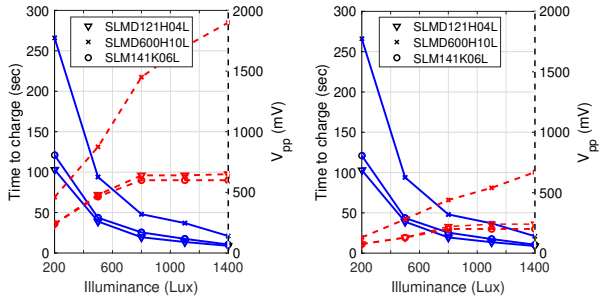

(a) LiFi at 50 kHz. **(b) LiFi at 100 kHz.**

Figure 9: Comparison of peak-to-peak voltage and time to charge 100µF capacitor for shortlisted solar cells at different LiFi transmission rates. For the three solar cell types the exposed area is 30 cm^2.

based on good performance both in communication, (V_{pp}), and in harvesting, time-to-charge.

Fig. 9 compares the three best solar cell types under evaluation. As the selected solar cells have different size, for carrying out a fair comparison, we connect several solar cell of each type in order to create the same total area. In total, we create a solar cell of approximately 3000 mm^2 by unifying 5, 4, 3 solar cells of 'SLMD121H04L', 'SLMD600H10L' and 'SLM141K06L', respectively. Following our analysis in Section 4.1, solar cells are connected in series for V_{pp} results, as the voltage in the output of each solar cell is summed up. Differently, they are connected in parallel for time-to-charge results, as the current in the output of each solar cell is added to contribute to a faster harvesting. We observe that time-to-charge monotonically decreases with illuminance, whereas V_{pp} monotonically increases with illuminance, which contributes to a faster harvesting and a better communication, respectively. However, the frequency of LiFi transmission does not affect the time-to-charge, but the V_{pp} decreases when LiFi rate increases due to the low bandwidth of the solar cell. In fact, the capacitance of solar cells distorts the received signal and, as a consequence, the V_{pp} value. In the next section, we search for a Pareto-optimal solution [27], as there is not a single solar cell type that provides the best performance in both communication and harvesting.

4.4 Criterion to choose the solar cell

The aim of this subsection is to choose the best solar cell type in terms of communication and harvesting. Communication is optimized by maximizing V_{pp}, i.e., minimizing $-V_{pp}$, while time to charge (T_c) is optimized by minimizing it. Fig. 10 shows the Pareto fronts for fixed illuminance and frequency, which demonstrates that the solar cell 'SLM141K06L' is Pareto-dominated by 'SLMD121H04L'. However, we observe that both 'SLMD121H04L' and 'SLM600H10L' are within the Pareto-front, which means that both are Pareto efficient. To select a single solar cell type as the best solar cell for our scenario, we convert the problem into a unique objective function to be minimized, by using the weighted sum method as

$$f_1 = \alpha \cdot T_{c,\text{norm}}(T, l, f) - (1 - \alpha) \cdot V_{pp,\text{norm}}(T, l, f), \qquad (1)$$

where α is the weight that is typically set by the decision maker, $T \in \{A, B, C\} = \{$'SLMD121H04L', 'SLM600H10L', 'SLM141K06L'$\}$

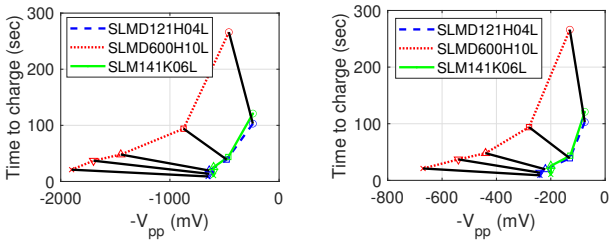

(a) LiFi at 50 kHz. (b) LiFi at 100 kHz.

Figure 10: Representation of Pareto fronts for each illuminance value when considering shortlisted solar cells at different LiFi transmission rates.

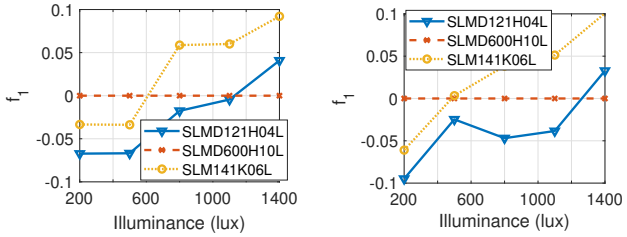

(a) f=**50 kHz,** $\alpha = 0.5$. (b) f=**100 kHz,** $\alpha = 0.5$.

Figure 11: Representation of function to minimize versus illuminance. The figure shows how the solar cell 'SLMD121H04L' provides the best performance both in communication and harvesting. Note that curve belonging to 'SLMD600H10L' is zero for all illuminance values because this solar cell achieves $T_{c,max}(l, f)$ and $V_{pp,max}(l, f)$ values.

represents the solar cell type, and l and f are the illuminance and LiFi frequency, respectively.

The computation of the optimal solar cell can be derived from the analysis we conduct in the Appendix. From there, Fig. 11 represents f_l for each solar cell type versus illuminance for 50 kHz and 100 kHz of transmission rate and considering $\alpha = 0.5$ (an equal importance for communication and harvesting). In such figure, solar cell 'SLMD121H04L' provides the lowest f_l value for typical lighting conditions in indoor environments [20] [30]. However, for larger illuminance values 'SLMD600H10L' becomes the best solar cell due to the larger differences in V_{pp} (see Fig. 9). Considering the results obtained in Fig. 11 and as illuminance values for indoor work places are typically lower than 1200 lux [20], the solar cell with the best harvesting and communication capability is 'SLMD121H04L'.

After the selection of the solar cell, we select the number of solar cells to use and their configuration. As the size of our prototype tag is 75 x 50 mm, and as the larger the number of solar cells, the better are communication and harvesting (see Fig. 7), we place 5 SLMD121H04L solar cells on the back side of the tag to fully cover the area, as shown in Fig. 1.

4.5 Receiver circuitry

As next step, the DC and AC components at the output of the solar cell are separated using low pass filter (LPF) and high pass filter (HPF) respectively, as shown in Fig. 12b. The photocurrent from solar cell consists of both AC (i_{sc}) and DC component (I_{sc}). The DC component is blocked by C_1 and passes through the branch for harvesting energy. The AC components flows through both the

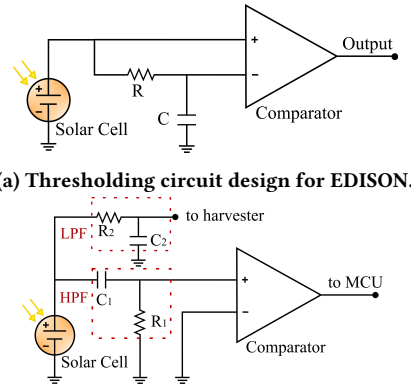

(a) Thresholding circuit design for EDISON.

(b) Proposed thresholding circuit.

Figure 12: Configuration of the thresholding circuit. We integrate LPF and HPF, for harvesting and communication purposes, respectively. This improves the robustness of the thresholding circuit.

branches but it is highly attenuated by C_2 [41]. The optimization of R_2 is important, and it causes a trade-off between communication range and time to charge. Larger the value of R_2 greater will V_{pp} and T_c be as shown in Fig. 13a. However, note that V_{pp} is not improved from a R_2 value on, whereas the time to charge keeps increasing. In order to find the optimal R_2 value to operate by optimizing both communication and harvesting simultaneously, we develop the same method as the one used for finding the optimal solar cell type. The optimal R_2 value is 4 kΩ, where V_{pp} starts saturating and from this point on the harvesting (time to charge) worsens dramatically. However, we identify that the optimum R_2 depends on the data rate: at low data rates (shown in Fig. 13a), V_{pp} is larger than $V_{pp,min}$ for all R_2 values.

For the sake of simplicity, unless other data is specified, from this point on, we will perform with the optimal solar cell and optimum R_2 value, i.e., solar cell type 'SLMD121H04L' and R_2 = 4 kΩ. The values of C_1 and R_1 are selected to rectify the low frequency noise from ambient lighting. Also, the HPF removes the DC component of the signal and translates signal down to ground as average.

4.6 Backscatter Circuitry

We describe the backscatter circuitry, referring to Fig. 14. The AC component of the received signal contains LiFi data and chirps. The chirps are originally transmitted by the LiFi infrastructure and received by the solar cell-based LiFi receiver. The optical chirps varying from frequency f_1 to f_2 are converted to electrical chirps by the solar cell and further processed by the HPF and comparator. The recovered chirps are fed into the RF switch to toggle the RF antenna between absorption and reflection state. The antenna mixes the chirps with RF carrier signal and backscatters the signal varying from f_c+f_1 to f_c+f_2.

5 EVALUATION

In this section we present the experimental evaluation of our design and comparison with state-of-the-art work. The results are focused on the following points:

- Ability of our end-to-end system to detect the chirps in CSS modulated signal below the noise floor. Our backscatter receiver shows detection of upchirps up to -17 dB below the noise floor.

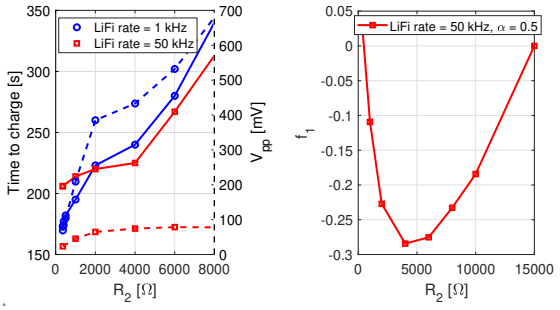

(a) Peak-to-peak voltage (dashed) and Time to charge (solid) for different R_2 values and LiFi rates.

(b) The optimal point for both communication and harvesting is $R_2 = 4\,\text{k}\Omega$, when LiFi rate = 50 kHz.

Figure 13: Calculation of the optimal R_2 value for both communication and harvesting functionalities when LiFi rate is 1 kHz and 50 kHz.

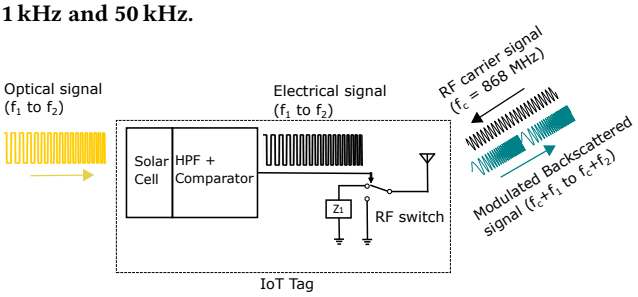

Figure 14: Scheme for mixing recovered chirp signal with RF carrier to enable uplink backscatter communication on tag.

- A 2x improvement in range of uplink communication in outdoor and indoor environment with 90% decrease in power consumption as compared to EDISON. Also, the range of communication with respect to the consumed power by the tag outperforms works like LoRa backscatter [34] and Lorea [39].
- Performance of system in terms of harvesting and LiFi downlink in indoor and outdoor environment.

5.1 Experimental setup

LiFi transmitter. In our LiFi transmitter, the baseband signal could be generated using the programmable real-time unit (PRU) of the Beaglebone used as embedded processor (similarly to OpenVLC). For generating the chirp signal, as proof of concept, we use the multi-function instrument Analog Discovery 2 to generate baseband signal with transmission structure shown in Fig. 15. The LiFi transmitter provides constant illumination. Downlink transmission implements Manchester coding to guarantee constant light level regardless of the bit stream. The LiFi transmitter communicates with the tag sending LiFi frame at the desired data rate with a packet structure that includes preamble, start frame delimiter (SFD), transmitter identifier, receiver identifier, frame length and payload. After the downlink frame, the transmitter recurrently sends up-chirp signal varying from a minimum frequency of 40 KHz to a maximum one of (40 + BW), where BW is the bandwidth of the chirp signal.

Tag. The received analog signal (LiFi frame and chirp) is digitized by using 1-bit ADC implemented using TS881 [33] comparator. The tag uses MSP430FR5969 [38] microcontroller unit (MCU) for

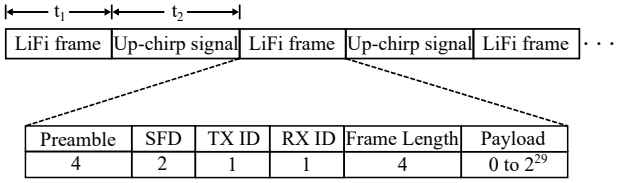

Figure 15: Transmission of LiFi frame and up-chirp signals (size of LiFi frame in bytes).

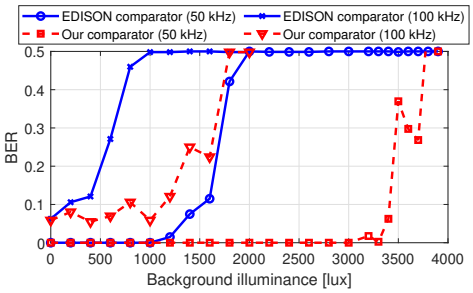

Figure 16: Thresholding circuit evaluation: BER versus background illuminance provided by an external unmodulated LED when LiFi transmission rate is 50 kHz and 100 kHz. The illuminance provided by the LiFi bulb is 550 lux in dark environment and at a distance between transmitter and receiver of 1.5 m.

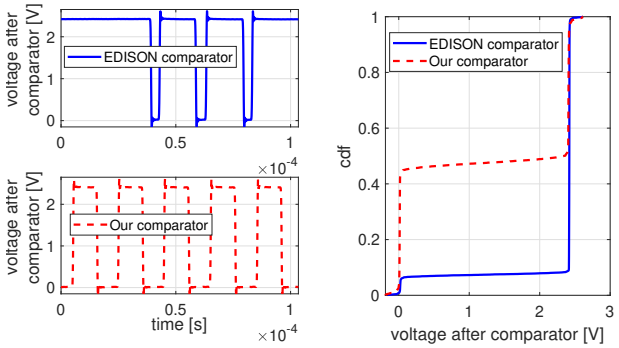

(a) Time-domain signals.

(b) CDF of signal values.

Figure 17: Time-domain signals after comparator when 50 kHz of LiFi transmission rate, 1.5 m of distance and 1800 lux of background light.

processing of LiFi received data. The tag wakes up when a preamble and SFD are detected, similarly to [12], else the tag stays in sleep mode. The energy harvesting is performed by solar cell combined with the Texas Instrument BQ25570 [37] integrated circuit to efficiently extract power from solar cell using Programmable Maximum Power Point Tracking (MPPT). The voltage at the output of harvester is regulated to 2.4 V using S-1313 [2] voltage regulator. For uplink communication, the multiplexer ADG704 [3] selects between chirp signal and Ground depending on uplink data '1' or '0' to transmit (e.g. directly received from the sensor), respectively. RF switch ADG902 [5] is used to vary the impedance of antenna to backscatter the 868 MHz carrier signal.

Carrier emitter and RF receiver. The uplink communication is established by backscattering the 868 MHz tone transmitted by

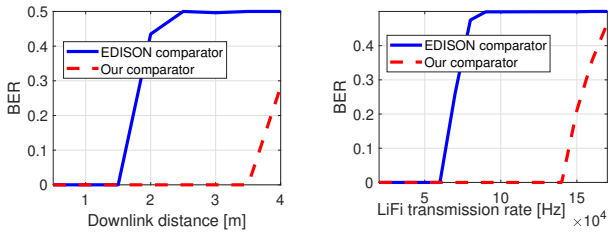

(a) BER versus distance. (b) BER versus LiFi rate.

Figure 18: Threshold circuit evaluation: BER versus distance (at 50 kHz of LiFi transmission rate) and BER versus LiFi transmission rate (at a distance of 1.5 m) with 800 lux background light.

the carrier wave (CW) generator. Any off-the-shelf modem or transmitter chipset can be used to generate the tone [16, 39]. In our experiments, we use two software defined radio USRPs B210 [10] to transmit the RF carrier at 868 MHz and receive the RF backscatter signal, respectively.

We use the open source standard compliant LoRa receiver for the detection of upchirps [23]. The design is implemented in Pothos flow software. To exploit the CSS synchronization method, we modify the receiver to detect one synchronization word that corresponds to one upchirp. Once synchronized, later upchirps are considered as data symbols. Then, note that although we invoke the CSS fundamentals of LoRa standard, we do not transmit standardized LoRa codewords. We rather exploit the CSS concept for increasing uplink distance. However, this could be implemented with a strict synchronization, at the expense of an increase in complexity.

5.2 LiFi Receiver

For our LiFi receiver, we observe three main findings. First, it is more robust to background illumination as shown in Fig. 16 with respect to prior work. The bit error rate (BER) is plotted against the background illuminance. The plot depicts the improved performance of our comparator design with 0% BER in presence of 1000 lux and 3000 lux when operating at 100 kHz and 50 kHz LiFi transmission frequency, respectively.

Second, the output of the comparator is independent from the input frequency and symmetry is maintained as shown in Fig. 17. This makes sampling of bits at the LiFi receiver less prone to error. Differently from our thresholding circuit, we notice that the duty cycle of signal after EDISON comparator is not 50%, and sometimes it is even 100%, which introduces a large number of errors in the decoding process.

Finally, the improvement in range is displayed in Fig. 18a. Our design can reach up to 3.5 m with 0% BER with a background of 800 lux. Fig. 18b shows the improvement in terms of data rate. Our system can achieve transmission frequency of 140 kHz corresponding to 280 kbps as compared to 120 kbps by EDISON design. As the data rate of LiFi transmitter increases, PassiveLiFi can better cope with capacitance effect from the solar cell, thanks to the higher symmetry and higher dynamic range of our LiFi transmitter, and higher robustness to noise of our passive LiFi receiver.

5.3 Uplink reception

We evaluate PassiveLiFi in terms of its ability to detect the chirps below the noise floor. The LiFi downlink generates the upchirps

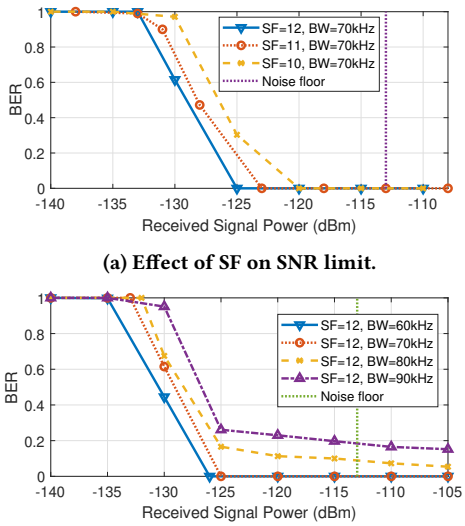

(a) Effect of SF on SNR limit.

(b) Effect of BW on SNR limit.

Figure 19: Evaluation of backscatter receiver to detect chirps below the noise floor.

at the tag which are used by the backscatter module to vary the antenna impedance. The distance between the tag and carrier wave generator is fixed at 1.4 m. Note that although we conduct experiments with a relative short range in LiFi link between the LED and the tag, we may require a long range for RF backscatter in order to transmit sensed data to the edge device. This enables to have a unique (or a few) edge devices for multiple rooms (indoors) or a large coverage area (outdoors). The transmission power of carrier generator is varied to evaluate system for different received power. The results are shown in Fig. 19 for OOK modulation scheme used in EDISON (demodulates only above noise floor), and CSS used in our design. Fig. 19a and Fig. 19b show the effect of spreading factor (SF) and bandwidth (BW) on SNR limit, respectively. With the increase of SF, the SNR limit decreases and with increase in BW, SNR limit increases which is consistent with LoRa standard. In the best configuration (SF 12 and BW 60 kHz), our receiver decodes 17 dB below the noise floor.

We are limited by the noise floor of the USRP. However, we can significantly improve the communication performance through the usage of commodity transceivers for reception which gives up to 25-30 dB lower noise floor when compared to the SDR [34]. The selection of chirp BW is important here, as on lower side we are limited by the interference from the carrier generator tone and on higher side limited by the BW of solar cell. For generating chirps we use 40 kHz as lower limit and upper limited is selected based on the value of chirp BW i.e. 100 kHz for chirp with 60 kHz BW. In Fig. 19b, with 90 kHz BW. it can be seen that the highest BER is 0.18 due to the limitation of solar cell's BW.

5.4 Uplink range and energy consumption

We evaluate the uplink range in both indoor and outdoor scenarios. In indoor environment, we perform the test inside a building in ground floor by keeping the tag and CW generator in a room at distance of 1.4 m. We place the RF receiver at position P1, P2, P3, P4, P5, P6, P7 at distance of 5.5, 13, 18, 23, 36, 40 and 47 m, respectively,

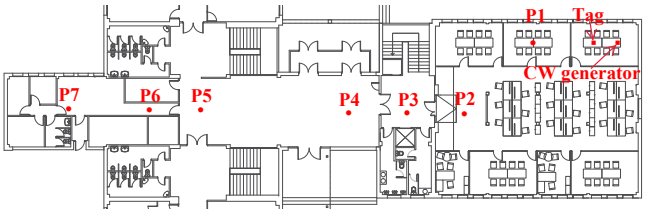

Figure 20: Plan of indoor scenario. Positions of tag and CW generator are highlighted, and positions of RF receiver are marked with P1-7.

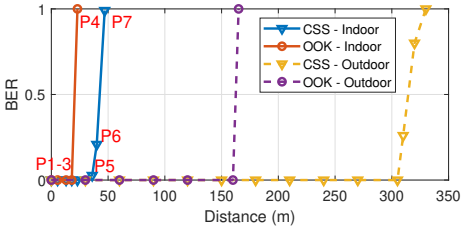

Figure 21: Range of tag at indoor and outdoor scenarios. Tag and CW generator are located at a distance of 1.4 for indoor and 1 m for outdoor, and the RF receiver is moved away.

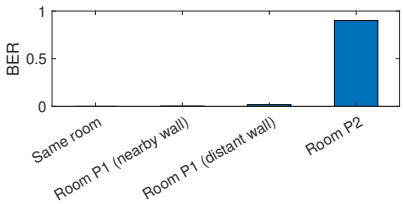

Figure 22: Range of tag when it is moved away while CW generator and RF receiver are placed at a different room at a distance of around 7 m from the tag.

from tag as shown in Fig. 20. As shown in Fig. 21, we observe a significant increase in range by PassiveLiFi as compared to EDISON. With our design, we get range as large as 40 m with normalized bit loss rate less than 0.20, which is 2x improvement over EDISON.

In outdoor scenario, we perform the experiment in an open space. We use the same configuration for tag and CW generator as in indoor and we place the backscatter receiver at different distances in open space. Note that outdoor light sources such as streetlights may be located at a larger distance, but their transmission power is also larger than the power of our LiFi transmitter, which enables these outdoor experiments. Thus, these outdoor results are still very valuable to evaluate. The results are presented in Fig. 21. We obtain around 2x improvement over EDISON, with range up to 305 m for our design. The energy consumption of backscatter module is significantly reduced by offloading the oscillators which are the most power hungry components in backscatter module. The energy is reduced from 70 µW (as in EDISON) to 3.8 µW. Only comparator, multiplexer and RF switch are the active elements in backscatter module with typical power consumption < 1 µW.

Table 1 presents a comparison in ratio between achieved distance over uplink consumption. Note that the reported effective isotropic radiated power (EIRP) is different at every state-of-the-art work, which is unfair. To make a fair comparison, we consider the Friis' path model to get the corresponding sensitivity of receivers. Knowing that and setting up the same EIRP as in our scenario (20 dBm),

Table 1: Computation of maximum achieved range versus uplink power consumption.

Lorea [39]			
EIRP	28 dBm	Max. dist.	Ratio
Max. distance	3.4 km	when 20 dBm:	distance-consumption:
Operation freq.	868 MHz	950 m	**13.6 m/μW**
Uplink consumption	70 μW		
Lora Backscatter [34]			
EIRP	36 dBm	Max. dist.	Ratio
Max. distance	2.8 km	when 20 dBm:	distance-consumption:
Operation freq.	915 MHz	435 m	**47 m/μW**
Uplink consumption	9.25 μW		
EDISON [12]			
EIRP	20 dBm		Ratio
Max. distance	160 m		distance-consumption:
Operation freq.	868 MHz		**2.29 m/μW**
Uplink consumption	70 μW		
PassiveLiFi (Proposal)			
EIRP	20 dBm		Ratio
Max. distance	305 m		distance-consumption:
Operation freq.	868 MHz		**80.3 m/μW**
Uplink consumption	3.8 μW		

we are able to compute the maximum achieved distance in uplink under same configuration. Note that the maximum distance considered for LoRea is the one that provides a BER=10^{-2} and 2.9 kbps, whereas the maximum distance considered for LoRa Backscatter is the one that obtains 200 bps. As seen in ratio distance-consumption results, our PassiveLiFi tag shows an uplink efficiency much larger (x2) than previous works, which makes it much more sustainable while achieving longer ranges.

Last indoor experiment demonstrates the possibility of locating the tag at a different room as CW generator and RF receiver. Fig. 22 shows that, when placing CW generator and RF receiver in same room at a distance of 2.3 m, the signal can be decoded when the tag is located at a different room at a distance of around 7 m. Unlike prior works [12], we enable the possibility of separating tag from either RF receiver or CW generator, increasing the flexibility of the setup indoors.

5.5 Harvesting and LiFi downlink

The energy harvested by the IoT tag and the BER in LiFi downlink are represented in Fig. 23a and Fig. 23b, respectively. We show the performance when the two configurations of solar cells are established. Note that, when solar cells are connected in series the achieved range may be increased due to providing a larger peak-to-peak voltage in the output of solar cells. However, at low LiFi rates this difference is not noticeable (subject to some minor experimental errors), because the speed response of solar cell does not clip the peak-to-peak voltage and then allowing to achieve similar results. Differently, the harvested energy provided by solar cells in parallel are always better than when they are connected in series. Then, at lower rates, it is better to configure solar cells in parallel, while at higher rates, it is convenient that connection in series and in parallel are switched adaptively to optimize decoding and harvesting, respectively.

5.6 Self-sustainability of tag

We study the self-sustainability of tag at different LiFi bit rates and present the results in Fig. 24. For this experiment, we optimize R_2 as

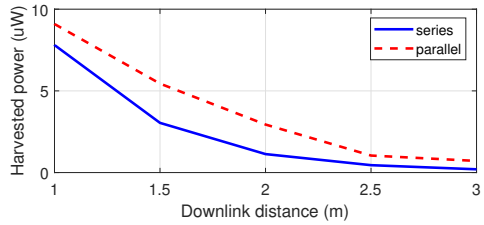

(a) Harvested power at different downlink distances when solar cells are connected in parallel or series.

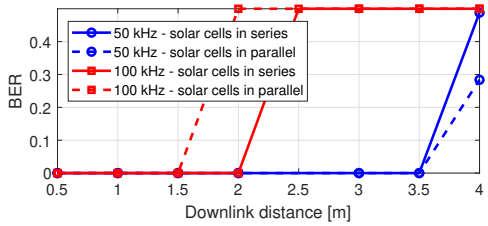

(b) BER at different downlink distances when solar cells are connected in parallel or series.

Figure 23: Evaluation of solar cells configuration. Energy harvesting improves with solar cells connected in parallel, while communication reliability improves with solar cells connected in series (lower BER, reliable link).

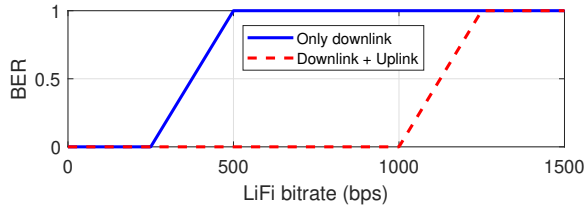

Figure 24: Self-sustainability of tag at 250 bps with continuous downlink without any intermittent behaviour. In case of both downlink and uplink sequentially, the tag achieves 1000 bps without outages to harvest energy at 500 lux.

explained in Sec. 4, i.e., R_2 is the lowest possible value that enables communication, then boosting harvested energy. Concretely, $R_2 = 350\Omega$ and LiFi transmitter and tag are separated by 1.5 m. Note as PassiveLiFi tag is self-sustainable at a LiFi bitrate of 250 bps (corresponding to 500 ksamples per second, due to the usage of Manchester coding to guarantee an equal number of high and low symbols) when constant LiFi frames are received. When a time-division duplexing is carried out for downlink (0.5 s) and uplink (1 s) transmission as specified in Fig. 15, the LiFi rate while guaranteeing self-sustainability of tag may increase up to 1 kbps thanks to the greater power efficiency of uplink communication.

6 APPLICATION SCENARIOS

There has been interest in IoT and mobile systems that leverage light and RF for sensing and communication. For example, LiFi systems are currently being deployed in large numbers to support high-speed downlink communication applications. These systems predominately use RF to support uplink transmissions, commonly through energy-expensive WiFi radios. Our system builds on these efforts and develops mechanisms to support energy-efficient uplink for battery-free devices through RF backscatter. LiFi for battery-free devices is largely unexplored, and our system targets this vital area and paves the way to enable numerous scenarios. We discuss some of these application scenarios.

Outdoor deployments. The deployment of sensors in outdoor settings enables numerous applications. For example, they may be deployed at a large scale to enable the concept of smart cities. These applications require a large deployment of sensors and these sensors transmit their information to a reasonably large range. Our system benefits from these scenarios, as most outdoor settings provide access to lighting infrastructure that could be re-purposed for delegation of the oscillations or to support downlink communication. Further, our system enables us to lower the complexity and power consumption of the tags, which is necessary for large-scale deployments in outdoor settings.

Smart homes. We are automating homes and deploying IoT devices in large numbers. Today, almost all of these IoT devices are energy-expensive and are reliant on batteries. Backscatter may help overcome this reliance. However, backscatter in devices deployed in homes is challenging due to lack of downlink communication and limited range. Our system is well suited for indoor environments as the artificial lighting is omnipresent indoors, providing a downlink channel to the backscatter tags. Further, the large communication range due to CSS can enable flexibility in the receiver-equipped edge device's placement. One main limitation of LiFi is that the best communication range is achieved on a Line-Of-Sight (LoS) link. However, the trend is toward deploying lighting infrastructure composed by dense light fixtures [7], where every point in the room is illuminated by more than one fixture in order to comply with lighting standards (illuminance homogeneity, average illuminance, etc.). This will ensure receiving a signal from more than one light fixture, which reduces enormously the blockage probability.

Farming. Growing plants in an indoor environment such as in greenhouses are attracting significant interest. These environments require a deployment of sensors to track soil moisture, temperature, etc. Further, artificial lighting is omnipresent to help plants grow. Our system could benefit such applications by taking advantage of already present lighting and enabling the low-cost and deployment of sensors that require lesser deployment efforts.

7 RELATED WORK

We discuss works that are most related to our system.

Backscatter Communication Recent systems show ability to synthesise transmissions compatible with WiFi [17], ZigBee [16], BLE [9], and LoRa [34], other systems have achieved an enormous communication range [34, 39]. It enables new scenarios and possibilities. However, backscatter systems have a poor ability to receive transmissions. These tags are limited due to the passive envelope detectors employed to perform reception. They suffer from poor sensitivity, susceptibility to cross-technology interference, and their inability to support complex modulation schemes. In this regard, we take a step to overcome these limitations by building on recent systems that advocate LiFi as an alternative to RF to receive downlink information [12, 13]. When compared to these systems, we significantly improve design, exploring the trade off between solar cell size, energy harvesting and communication, improve the robustness of the LiFi receiver through various energy-efficient filters

and the RF backscatter ability by leveraging chirp spread spectrum scheme enabled through the concept of LiFi as an oscillator.

Offloading Computing, Processing and Oscillations The past decade has seen a dramatic improvement in the energy efficiency of sensors, with microphones [35] and cameras [28] consuming tens of microwatts of power. It has made computation and communication significantly more energy expensive than sensing. Backscatter reduces this energy asymmetry, as it brings the energy cost for performing transmissions to a level similar to that for performing sensing. Consequently, computational elements such as FPGAs and MCUs are a crucial bottleneck. Recent systems have advocated eliminating computational elements. They couple the sensor directly to a backscatter transmitter and delegate all the necessary sensor readings to a powerful edge device. Building on this architecture: [35] designs a battery-free cellphone that transmits audio signals. Further, recent systems even demonstrate battery-free video streaming cameras [28].

Recent systems have explored delegating oscillators to externally powered infrastructure. [31] generates a twin carrier tone by repurposing a WiFi device. This enables them to provide energy expensive oscillations to a tag. We build on these insights and delegate the energy expensive oscillations to the infrastructure. Our work differs in using LiFi signals to deliver oscillations. Our work is most closely related to EDISON [12], which has shown in a dedicated experiment the possibility to deliver clock signals through light. As shown in our evaluation, we significantly improve their design by enhancing the LiFi transmitter and receiver and demonstrating the ability to receive chirps signals, thus broadly improving the overall performance.

There have also been efforts to recover clock signals from optical communication, leading to energy-efficient integrated circuits (IC). In particular, some of these systems demonstrate recovery of clock signals from the Manchester encoded data using low-power digital circuits [42][22]. Our system is complementary to these systems, and goes much beyond the capabilities demonstrated by prior designs. We demonstrate the recovery of complex baseband signals that employ a complex chirp spread spectrum (CSS) modulation scheme, which we then used to modulate an RF carrier. Nevertheless, we can also employ techniques presented in prior works to improve our system's energy efficiency, helping us realise low-power ICs.

Solar cell for LiFi. Solar cells have seen interest beyond their traditional role of harvesting energy from light. There has been an effort to repurpose them for LiFi communication. It has enabled a significant reduction in the energy consumption of the LiFi frontend. Some works have designed application-specific integrated circuits [42] [21] which are difficult to replicate or use in a different context, such as low-power backscatter communication. Other systems have only used solar cells for harvesting or communication, and they lack the necessary design to optimise for both energy harvesting and communication [25] [41]. As opposed to these systems, we design a low-power mechanism that can harvest and communicate using the LiFi infrastructure and enable various applications.

LiFi Communication for IoT devices Active LiFi aims to create a networked system that uses modulated light bulbs and active receivers. More and more often, uplink communication relies on RF [15]. However, these systems use energy-expensive components, which pushes them beyond the means of IoT devices. Recent systems have tackled the challenge of LiFi on battery-free devices. RetroVLC and PassiveVLC demonstrate a battery-free tag that can receive downlink transmissions using LiFi and uplink through visible light backscatter [18, 44]. [43] builds on these systems and improve the throughput and range of visible light backscatter systems. However, these systems suffer from the challenge of directionality of visible light backscatter links. Further, their downlink LiFi reception suffered from challenges of ambient noise. We design an efficient LiFi receiver. Further, we adopt the EDISON approach of using RF backscatter to support uplink transmissions and significantly improve their design by using chirps to improve the range. We expect that RF (backscatter) will likely become the predominant technology for uplink communication and passive LiFi.

8 CONCLUSION

We have presented PassiveLiFi. It explores the interactions between LiFi downlink and RF backscatter uplink to achieve very low-power and long-range uplink communication. Our design introduces visible light chirps that are sent by the LiFi transmitter, which are received and mixed by the IoT tag with the input RF carrier to transmit uplink RF backscatter signals. We have extensively evaluated our system and shown promising results in reducing power consumed by the tag (3.8 μW) while communicating at a distance of up to 305 m using an RF carrier emitting at 17 dBm.

9 ACKNOWLEDGMENTS

This work has been funded by the European Union's Horizon 2020 research and innovation programme under the Marie Skłodowska Curie grant agreement ENLIGHTEM No. 814215. Besides, this work has been partially funded by Juan de la Cierva Formación grant (FJC2019-039541-I / AEI / 10.13039/501100011033) granted to author B. Genoves Guzman, and Vinnova (Sweden Innovation Agency) under the grant (2018-04305) awarded to Ambuj Varshney.

APPENDIX

As variables T_c and V_{pp} have different ranges, they must be normalized to get $T_{\text{c,norm}}(T,l,f) = \frac{T_c(T,l,f)}{T_{\text{c,max}}(l,f)}$ and $V_{\text{pp,norm}}(T,l,f) = \frac{V_{\text{pp}}(T,l,f)}{V_{\text{pp,max}}(l,f)}$, respectively, where $T_{\text{c,max}}(l,f)$ and $V_{\text{pp,max}}(l,f)$ are the maximum $T_c(l,f)$ and $V_{\text{pp}}(l,f)$ values for such illuminance l and LiFi frequency f. Note that $T_{\text{c,max}}(l,f)$ ($V_{\text{pp,max}}(l,f)$) also corresponds to the $T_c(l,f)$ ($V_{\text{pp}}(l,f)$) value whose $V_{\text{pp}}(l,f)$ ($T_c(l,f)$) is maximum (minimum) [26].

The optimal solar cell type can be finally formulated as

$$T(l,f) = \begin{cases} A, & \text{if } \{V_{\text{pp}}(B,l,f), V_{\text{pp}}(C,l,f)\} < V_{\text{pp,min}} \\ B, & \text{if } \{V_{\text{pp}}(A,l,f), V_{\text{pp}}(C,l,f)\} < V_{\text{pp,min}} \\ C, & \text{if } \{V_{\text{pp}}(A,l,f), V_{\text{pp}}(B,l,f)\} < V_{\text{pp,min}} \\ \underset{T\in\{A,B,C\}}{\arg\min}\ f_1, & \text{otherwise} \end{cases} \quad (2)$$

where $V_{\text{pp,min}}$ is the minimum V_{pp} value required for decoding the data correctly. Due to experiments, we conclude that $V_{\text{pp,min}}$ = 30 mV, i.e., this is the minimum V_{pp} value required for decoding the signal on the tag. As can be seen in Fig. 9 and Fig. 10, under low illuminance conditions in our setup, V_{pp} is still above $V_{\text{pp,min}}$. This simplifies (2) as

$$T(l,f) = \underset{T\in\{A,B,C\}}{\arg\min}\ f_1. \quad (3)$$

REFERENCES

[1] LoRa Alliance. https://lora-alliance.org/.

[2] Ablic. S-1313. https://www.ablic.com/en/doc/datasheet/voltage_regulator/S1313_E.pdf.

[3] Analog Devices. ADG704. https://www.analog.com/media/en/technical-documentation/data-sheets/adg704.pdf.

[4] Analog Devices. ADG72X switches. https://www.analog.com/media/en/technical-documentation/data-sheets/adg721_722_723.pdf.

[5] Analog Devices. ADG902. https://www.analog.com/media/en/technical-documentation/data-sheets/adg901_902.pdf.

[6] M. Anderson. Potential Hazards at Both Ends of the Lithium-Ion Life Cycle. *IEEE Spectrum*, 2013.

[7] J. Beysens, A. Galisteo, Q. Wang, D. Juara, D. Giustiniano, and S. Pollin. DenseVLC: A Cell-Free Massive MIMO System with Distributed LEDs. In *Proceedings of the 14th International Conference on Emerging Networking EXperiments and Technologies*, CoNEXT '18, page 320–332, New York, NY, USA, 2018. Association for Computing Machinery.

[8] J. de Winkel, V. Kortbeek, J. Hester, and P. Pawełczak. Battery-free game boy. *Proc. ACM Interact. Mob. Wearable Ubiquitous Technol.*, 4(3), Sept. 2020.

[9] J. F. Ensworth and M. S. Reynolds. Every smart phone is a backscatter reader: Modulated backscatter compatibility with bluetooth 4.0 low energy (BLE) devices. In *2015 IEEE international conference on RFID (RFID)*, pages 78–85. IEEE, 2015.

[10] Ettus Research. USRP B210. https://www.ettus.com/wp-content/uploads/2019/01/b200-b210_spec_sheet.pdf.

[11] A. Galisteo, D. Juara, and D. Giustiniano. Research in visible light communication systems with OpenVLC1.3. In *Proc. IEEE WF-IoT*, 2019.

[12] A. Galisteo, A. Varshney, and D. Giustiniano. Two to tango: Hybrid light and backscatter networks for next billion devices. In *Proceedings of the 18th International Conference on Mobile Systems, Applications, and Services*, MobiSys '20, page 80–93, New York, NY, USA, 2020. Association for Computing Machinery.

[13] D. Giustiniano, A. Varshney, and T. Voigt. Connecting Battery-Free IoT Tags Using LED Bulbs. In *Proceedings of the 17th ACM Workshop on Hot Topics in Networks*, HotNets '18, page 99–105, New York, NY, USA, 2018. Association for Computing Machinery.

[14] M. Gorlatova, J. Sarik, G. Grebla, M. Cong, I. Kymissis, and G. Zussman. Movers and shakers: Kinetic energy harvesting for the internet of things. *IEEE Journal on Selected Areas in Communications*, 33(8):1624–1639, 2015.

[15] H. Haas, L. Yin, C. Chen, S. Videv, D. Parol, E. Poves, H. Alshaer, and M. S. Islim. Introduction to indoor networking concepts and challenges in LiFi. *IEEE/OSA Journal of Optical Communications and Networking*, 12(2):A190–A203, 2020.

[16] V. Iyer, V. Talla, B. Kellogg, S. Gollakota, and J. Smith. Inter-technology backscatter: Towards internet connectivity for implanted devices. In *Proceedings of the 2016 ACM SIGCOMM Conference*, pages 356–369, 2016.

[17] B. Kellogg, V. Talla, S. Gollakota, and J. R. Smith. Passive Wi-Fi: Bringing Low Power to Wi-Fi Transmissions. In *NSDI'16*, Berkeley, CA, USA, 2016. USENIX.

[18] J. Li, A. Liu, G. Shen, L. Li, C. Sun, and F. Zhao. Retro-VLC: enabling battery-free duplex visible light communication for mobile and IoT applications. In *Proceedings of the 16th International Workshop on Mobile Computing Systems and Applications*, pages 21–26. ACM, 2015.

[19] Y. Li, T. Li, R. A. Patel, X.-D. Yang, and X. Zhou. Self-powered gesture recognition with ambient light. In *Proceedings of the 31st Annual ACM Symposium on User Interface Software and Technology*, pages 595–608, 2018.

[20] C. Light. Lighting—lighting of work places—part 1: Indoor work places. *European Committee for Standardization, Brussels, Belgium*, 2002.

[21] J. Lim, E. Moon, M. Barrow, S. R. Nason, P. R. Patel, P. G. Patil, S. Oh, I. Lee, H.-S. Kim, D. Sylvester, D. Blaauw, C. A. Chestek, J. Phillips, and T. Jang. 26.9 A 0.19×0.17mm2 Wireless Neural Recording IC for Motor Prediction with Near-Infrared-Based Power and Data Telemetry. In *2020 IEEE International Solid- State Circuits Conference - (ISSCC)*, pages 416–418, 2020.

[22] W. Lim, T. Jang, I. Lee, H.-S. Kim, D. Sylvester, and D. Blaauw. A 380pW dual mode optical wake-up receiver with ambient noise cancellation. In *2016 IEEE Symposium on VLSI Circuits (VLSI-Circuits)*, pages 1–2, 2016.

[23] LoRa modem with LimeSDR. https://github.com/myriadrf/lora-sdr.

[24] X. Lu, P. Wang, D. Niyato, D. I. Kim, and Z. Han. Wireless Networks With RF Energy Harvesting: A Contemporary Survey. *IEEE Communications Surveys Tutorials*, 17(2):757–789, 2015.

[25] S. Ma, F. Zhang, H. Li, F. Zhou, Y. Wang, and S. Li. Simultaneous lightwave information and power transfer in visible light communication systems. *IEEE transactions on wireless communications*, 18(12):5818–5830, 2019.

[26] J. Marler, R.T.; Arora. *Review of Multi-Objective Optimization Concepts and Methods for Engineering*. University of Iowa, Optimal Design Laboratory, Iowa City, IA. 2003.

[27] R. Marler and J. Arora. Survey of multi-objective optimization methods for engineering. *Structural and Multidisciplinary Optimization*, 26:369–395, 2004.

[28] S. Naderiparizi, M. Hessar, V. Talla, S. Gollakota, and J. R. Smith. Towards battery-free HD video streaming. In *15th USENIX Symposium on Networked Systems Design and Implementation (NSDI'18)*, pages 233–247, 2018.

[29] R. Nandakumar, V. Iyer, and S. Gollakota. 3D localization for sub-centimeter sized devices. In *Proceedings of the 16th ACM Conference on Embedded Networked Sensor Systems*, pages 108–119, 2018.

[30] I. E. S. of North America. *Lighting handbook: Reference & application*. Illuminating Engineering Society of North America, 2000.

[31] M. Rostami, K. Sundaresan, E. Chai, S. Rangarajan, and D. Ganesan. Redefining passive in backscattering with commodity devices. In *Proceedings of the 26th Annual International Conference on Mobile Computing and Networking*, pages 1–13, 2020.

[32] A. Saffari, M. Hessar, S. Naderiparizi, and J. R. Smith. Battery-free wireless video streaming camera system. In *2019 IEEE International Conference on RFID (RFID)*, pages 1–8, 2019.

[33] STMicroelectronics. TS881. https://www.st.com/resource/en/datasheet/ts881.pdf.

[34] V. Talla, M. Hessar, B. Kellogg, A. Najafi, J. R. Smith, and S. Gollakota. LoRa Backscatter: Enabling The Vision of Ubiquitous Connectivity. *Proc. ACM Interact. Mob. Wearable Ubiquitous Technol.*, 1(3):105:1–105:24, Sept. 2017.

[35] V. Talla, B. Kellogg, S. Gollakota, and J. R. Smith. Battery-free cellphone. *Proceedings of the ACM on Interactive, Mobile, Wearable and Ubiquitous Technologies*, 1(2):1–20, 2017.

[36] M. M. Tentzeris, A. Georgiadis, and L. Roselli. Energy harvesting and scavenging. *Proc. IEEE*, 102(11), 2014.

[37] Texas Instruments. bq25570. http://www.ti.com/lit/ds/symlink/bq25570.pdf.

[38] Texas Instruments. MSP430FR5949. http://www.ti.com/lit/ds/symlink/msp430fr5949.pdf.

[39] A. Varshney, O. Harms, C. Pérez-Penichet, C. Rohner, F. Hermans, and T. Voigt. LoRea: A Backscatter Architecture That Achieves a Long Communication Range. In *Proceedings of the 15th ACM Conference on Embedded Network Sensor Systems*, SenSys '17, pages 18:1–18:14, New York, NY, USA, 2017. ACM.

[40] A. Varshney, A. Soleiman, L. Mottola, and T. Voigt. Battery-free visible light sensing. In *Proceedings of the 4th ACM Workshop on Visible Light Communication Systems*, VLCS '17, pages 3–8, New York, NY, USA, 2017. ACM.

[41] Z. Wang, D. Tsonev, S. Videv, and H. Haas. On the design of a solar-panel receiver for optical wireless communications with simultaneous energy harvesting. *IEEE Journal on Selected Areas in Communications*, 33(8):1612–1623, 2015.

[42] X. Wu, I. Lee, Q. Dong, K. Yang, D. Kim, J. Wang, Y. Peng, Y. Zhang, M. Saligane, M. Yasuda, K. Kumeno, F. Ohno, S. Miyoshi, M. Kawaminami, D. Sylvester, and D. Blaauw. A 0.04MM316NW Wireless and Batteryless Sensor System with Integrated Cortex-M0+ Processor and Optical Communication for Cellular Temperature Measurement. In *2018 IEEE Symposium on VLSI Circuits*, pages 191–192, 2018.

[43] Y. Wu, P. Wang, K. Xu, L. Feng, and C. Xu. Turboboosting visible light backscatter communication. In *Proceedings of the Annual Conference of the ACM Special Interest Group on Data Communication on the Applications, Technologies, Architectures, and Protocols for Computer Communication*, SIGCOMM '20, page 186–197, New York, NY, USA, 2020. Association for Computing Machinery.

[44] X. Xu, Y. Shen, J. Yang, C. Xu, G. Shen, G. Chen, and Y. Ni. PassiveVLC: Enabling Practical Visible Light Backscatter Communication for Battery-free IoT Applications. In *Proceedings of the 23rd Annual International Conference on Mobile Computing and Networking*, MobiCom '17, pages 180–192, New York, NY, USA, 2017. ACM.

[45] Y. Zhang, Y. Iravantchi, H. Jin, S. Kumar, and C. Harrison. Sozu: Self-powered radio tags for building-scale activity sensing. UIST '19, page 973–985, New York, NY, USA, 2019. Association for Computing Machinery.